Supporting Information

Wang et al. 10.1073/pnas.1119073109

SI Methods

Sample Preparation and Definition of Constructs. Plasmids encoding KIX, TAZ1, TAZ2, and NCBD were generously provided by P. Wright (The Scripps Research Institute, La Jolla, CA). KIX was expressed and purified as described previously (1), whereas TAZ1, TAZ2, and NCBD were subcloned into pGEX4T-1 and purified using glutathione-Sepharose followed by Superdex 75 gel filtration (GE Healthcare). FOXO3a CR2C (M462-D483), CR3 (L620-A635), and CR2C-CR3 were cloned into pGEX4T-1 vector and then expressed and purified as described previously (1). All mutants were generated using QuikChange site-directed mutagenesis (Stratagene). The following provides a description of all constructs used in this study:

KIX: KIX domain of murine CBP (G586-L672) in pET21a vector
KIX MLL_{mut}: KIX with two mutations that disrupt the MLL site (I660A and L664A)
KIX c-Myb_{mut}: KIX with three mutations that disrupt the c-Myb site (Y650A, A654Q, and Y658A)
KIX $double_{mut}$: KIX with five mutations that disrupt both the MLL and c-Myb sites (I660A, L664A, A654Q, Y650A, and Y658A)
TAZ1, TAZ2, and NCBD: TAZ1 (A340-R439), TAZ2 (S1764-Q1855), and NCBD (P2059-Q2117) domains of murine CBP subcloned into pGEX4T-1 vector using the BamHI and Xhol sites
p300: Flag-tagged full-length human p300
p300 MLL_{mut}: Full-length p300 with two mutations that disrupt the MLL site of the KIX domain (I640A and L644A, equivalent to the mutations in KIX MLL_{mut})
p300 c-Myb_{mut}: p300 with three mutations in the c-Myb site (Y630A, A634Q, and Y638A)
p300 $double_{mut}$: p300 with five mutations that disrupt both the MLL and c-Myb sites (I640A, L644A, Y630A, A634Q, and Y638A)
p300 ΔN: p300 T1032-H2414
p300 ΔC: p300 M1-Q1736
CR2C: FOXO3a CR2C (M462-D483) in pGEX4T-1 vector
CR3: FOXO3a CR3 (L620-A635) in pGEX4T-1 vector
$CR3_{Trp}$: CR3 with the insertion of a Trp residue at the N terminus (W-L620-A635) in pGEX4T-1 vector
pCR3: Synthetic $CR3_{Trp}$ peptide with S626 phosphorylated (LifeTein)
$CR2C_{mut}$: CR2C with L474A mutation
$CR3_{mut}$: CR3 with I627A and I628A mutations
$CR3_{Trpmut}$: $CR3_{Trp}$ with I627A and I628A mutations
CR2C-CR3: Fusion of CR2C and CR3 connected by an engineered flexible linker (M462-D483)-$(GGGS)_3$-CR3(L620-A635), constructed by subcloning a synthetic gene (Genscript) into pGEX 4T-1 vector
CR2C-$CR3_{native}$: FOXO3a residues M462-A635 in pGEX4T-1 vector (peptide products released by thrombin cleavage of all constructs expressed from pGEX vectors contain a vector-encoded N-terminal Gly-Ser sequence)
Firefly luciferase: Firefly luciferase gene ligated to a promoter containing five GAL4 binding sites (2)
GAL4 DBD: GAL4 DBD (M1-S147) in pCMX vector
GAL4 fusion constructs: GAL4-CR2A-CR2B, GAL4-CR2C, GAL4-CR3, GAL4-$CR3_{mut}$, GAL4-CR2C-CR3, GAL4-$CR2C_{mut}$-CR3, GAL4-CR2C-$CR3_{mut}$, and GAL4-$CR2C_{mut}$-$CR3_{mut}$ are GAL4 DBD fused with the corresponding FOXO3a segments
GAL4-CR2C-CR3 SD: Contains the phosphomimetic mutation S626D
GAL4-CR2C-CR3L: GAL4 DBD-CR2C-$(GGGS)_9$-CR3
GAL4-CR2C-$CR3_{native}$: GAL4 DBD fused to FOXO3a residues (M462-A635)
GAL4-CR2A-CR2B: GAL4 DBD fused to FOXO3a CR2A and CR2B (T331-D340)-GGG-(L378-L390)
FOXO3aTM-ER: HA-tagged full-length FOXO3a-triple mutant (TM)-ligand binding domain of ER fusion protein bearing T32A, S253A, and S315A mutations, which block Akt phosphorylation-dependent cytoplasmic translocation
FOXO3aTM-ER bearing mutations in CR2C and/or CR3 designated as above (FOXO3aTM-ER $CR2C_{mut}$: FOXO3aTM-ER with L474A mutation in CR2C; FOXO3aTM-ER $CR3_{mut}$: FOXO3aTM-ER with I627A and I628A mutations in CR3; and FOXO3aTM-ER $double_{mut}$: FOXO3aTM-ER with L474A in CR2C and I627A and I628A in CR3).

Isothermal Titration Calorimetry. Calorimetric titrations were carried out on a Microcal VP-ITC titration calorimeter and were analyzed using a "one set of similar binding sites" model with the Origin software (MicroCal). The samples were prepared in NMR buffer at a concentration of 50 μM (sample cell) or 1–2 mM (syringe). The CR3 construct used for ITC has one Trp residue inserted after the pGEX vector-encoded Gly-Ser, which enabled UV spectrophotometric determination of peptide concentration.

NMR Spectroscopy. All NMR samples were prepared in 20 mM MES (pH 6.0) and 100 mM NaCl, except TAZ1, TAZ2, and NCBD, which were prepared in 20 mM Tris (pH 7.8), 100 mM NaCl, and 2 mM DTT. NMR data were acquired at 30 °C on Bruker Avance III 600-MHz and Avance II 800-MHz spectrometers, equipped with a 1.7-mm TCI MicroCryoProbe and a 5-mm TCI CryoProbe, respectively. Backbone assignments were achieved using standard ^{1}H-^{15}N-HSQC (3), HNCO (4), CBCA(CO)NH (5), and HNCACB (6) experiments. Side-chain assignments were obtained from ^{1}H-^{13}C-HSQC (7), HBHA(CO)NH (8), H(C)CH-COSY (9), and H(C)CH-TOCSY (τ_m = 21.7 ms) (10), and aromatic side chains of KIX were assigned using (HB)CB(CGCD)HD and (HB)CB(CGCDCE)HE NMR experiments (11). ^{1}H-^{15}N NOESY-HSQC (τ_m = 120 ms for KIX and τ_m = 100 ms for FOXO3a peptides) (12) and ^{1}H-^{13}C NOESY-HSQC (τ_m = 120 ms) (13) were recorded to confirm the assignments and provide NOE restraints for structure calculation. Intermolecular NOEs between KIX and CR2C-CR3 fusion peptide were identified by $^{13}C/^{15}N$-filtered (F1) ^{13}C-edited (F2) NOESY-HSQC spectra (τ_m = 120 ms) (14). Spectra were processed by NMRPipe (15) and visualized by NMRView (16), and resonances were assigned using XEASY (17). For NMR titrations, the normalized chemical shift changes were calculated using the equation $\Delta\text{Chemical shift} = \sqrt{[(\Delta H)^2 + (\Delta N/6.5)^2]}$.

Structure Calculation. CR2C-CR3 binds to KIX in two distinct orientations, and both structures were calculated using a strategy that involved collecting intramolecular NOEs for CR2C and CR3 bound to KIX MLL_{mut} and KIX c-Myb_{mut}, as well as intermolecular NOEs for CR2C-CR3 in complex with WT KIX domain, as illustrated in Fig. S4. The structure of the KIX do-

main was determined on the basis of manually assigned and CYANA (18) auto-assigned NOE distance constraints from ^{15}N- and ^{13}C-edited NOESY spectra of double-labeled KIX complexed with unlabeled CR2C-CR3, dihedral constraints from TALOS+ (19), and H-bond constraints based on chemical shift index, (20) together with the previously reported structure of KIX in complex with MLL and c-Myb peptides (PDB ID code 2AGH). Next, the structures of the KIX-bound conformations of CR2C and CR3 were determined, taking advantage of the KIX mutants MLL_{mut} and c-Myb_{mut}, each of which has only a single functional binding site. These mutants were designed based on a previous report (21) and our NMR titrations (Fig. S2*B*), and they were shown to disrupt the MLL and c-Myb sites, respectively, effectively (Table 1). We collected ^{15}N-edited NOESY spectra of complexes of double-labeled CR2C + KIX MLL_{mut}, double-labeled CR2C + KIX c-Myb_{mut}, double-labeled CR3 + KIX MLL_{mut}, and double-labeled CR3 + KIX c-Myb_{mut} (each sample contained a 2-fold excess of unlabeled KIX). The structures of CR2 and CR3 bound to KIX in the 2b3l mode were determined using NOE distance constraints derived from NOESY data of double-labeled CR2C + KIX MLL_{mut} and double-labeled CR3 + KIX c-Myb_{mut}, as well as chemical shift-based dihedral angle constraints from TALOS+. Finally, H-bond constraints were added using information from the preliminary structure. The structures of CR2 and CR3 bound to KIX in the 2l3b mode were determined in the same way using double-labeled CR2C + KIX c-Myb_{mut} and double-labeled CR3 + KIX MLL_{mut}. Intermolecular NOEs to determine the structure of the two complexes were obtained from filtered NOESY spectra of double-labeled CR2C-CR3 in the presence of a small excess of unlabeled KIX and double-labeled KIX with excess unlabeled CR2C-CR3. To calculate the complex structure, KIX and FOXO3a peptide were treated as a single chain connected by an artificial linker and the constraints already obtained for KIX and FOXO3a peptides were applied. A number of manually assigned intermolecular NOE distance constraints consistent with the 2b3l complex were used to guide CYANA to assign other 2b3l intermolecular NOEs automatically. This process was repeated for the 2l3b mode, and CYANA was used to build models of the two complexes. In the first run, 33 NOE peaks were used by CYANA as restraints in both the 2b3l and 2l3b structures, which may have resulted from similar chemical shifts or overlapped NOE signals. To validate our structures, we repeated the CYANA calculation after removing these peaks and found no substantial change in the structures. Finally, manual inspection of these 33 peaks allowed some of them to be assigned to either the 2b3l or the 2l3b structure, and the remaining ambiguous peaks were not used in the final structure calculations. The final structures were refined in explicit solvent using RECOORD (22) and analyzed using PROCHECK-NMR (23).

Cell Culture and Luciferase Assays. HEK 293T cells were maintained in DMEM supplemented with 10% (vol/vol) FBS, and the HCT116 Δp300 cells were cultured in McCoy's 5a Medium + 10% (vol/vol) FBS + 100 units/mL penicillin and streptomycin (GIBCO). For luciferase assays, plasmids were transfected using lipofectamine LTX (Invitrogen). The amounts of luciferase, GAL4 fusion, and p300 plasmids used in all the assays were 0.2, 0.4, and 0.8 μg per 3.5-cm well, respectively. Luciferase assays were performed using the Luciferase Assay System (Promega) with a SpectraMax M5 luminometer (Molecular Devices) 24 h after transfection. The amount of cell lysate used in each assay was normalized by total protein concentration measured by Bradford assay (Bio-Rad).

qRT-PCR. Primary MEFs transformed by E1a/Ras G12V were transfected with pIRES2/HA-FoxO3aTM-ER/EGFP (WT and mutants) (24), and stably transformed cells were obtained by G418 selection. To concentrate cells with high expression of the transgene, strong GFP-positive cells were further selected by cell sorting (25). Cells were seeded in DMEM containing 10% (vol/vol) dialyzed FBS and then treated with 0.5 μM 4-OHT. Total RNA was prepared after 4 and 8 h post-4OHT-treatment and purified using a Nucleospin RNA II kit (Macherey–Nagel) according to the manufacturer's protocol. Purified RNA was treated with DNaseI and reverse-transcribed using an iScript cDNA Synthesis Kit (Bio-Rad). cDNAs were subjected to real-time qRT-PCR using SYBR Green PCR Master Mix (Applied Biosystems). Primers used for qRT-PCR are as follows: β-actin, 5′-TTGCTGACAGGATGCAGAAG-3′ and 5′-ACATCTGCTGGAAGGTGGAC-3′; cyclophilin B, 5′-TGCAGGCAAAGACACCAATG-3′ and 5′-GTGCTCTCCACCTTCCGTA-3′; Bim, 5′-CGGATCGGAGACGAGTTCA-3′ and 5′-TTCAGCCTCGCGGTAATCA-3′; Cyclin G2, 5′-AGGGGTTCAGCTTTTCGGATT-3′ and 5′- AGTGTTATCATTCTCCGGGGTAG-3′; DDB1, 5′-GTGGGAATGTACGGGAAGATTG-3′ and 5′-CGCCACTCTGCTTATACTCCAA-3′; GADD45, 5′-CGCACTTGCAATATGACTTTG-3′ and 5′-GTACACGCCGACCGTAATG-3′; p27, 5′-CCTGACTCGTCAGACAATCC-3′ and 5′-TCTGTTCTGTTGGCCCTTTT-3′; Pck2, 5′-ATGGCTGCTATGTACCTCCC-3′ and 5′-GCGCCACAAAGTCTCGAAC-3′; PUMA, 5′-TCACCCTGGAGGGTCATGTA-3′ and 5′-GCGGGTGTAGGCACCTAGT-3′; FasL, 5′-TGGTTGGAATGGGATTAGGA-3′ and 5′-TACTGGGGTTGGCTATTTGC-3′; p21, 5′-CCACTTTGCCAGCAGAATAA-3′ and 5′-ACGGGACCGAAGAGACAAC-3′; and G6PC, 5′-CGACTCGCTATCTCCAAGTGA-3′ and 5′-GTTGAACCAGTCTCCGACCA-3′.

CD Spectroscopy. Far-UV CD spectra were recorded at 20 °C on a Jasco J-810 CD spectrometer at a scan rate of 20 nm/min. Data were collected in 1-nm increments from 200 to 250 nm, using a 0.1-cm path length cell and 8-s averaging time. Samples were prepared in the same buffer used for NMR, at a concentration of 1 mg/mL. The spectra were corrected by subtracting the spectrum of buffer.

1. Wang F, et al. (2009) Synergistic interplay between promoter recognition and CBP/p300 coactivator recruitment by FOXO3a. *ACS Chem Biol* 4:1017–1027.
2. Zhang J, Kalkum M, Yamamura S, Chait BT, Roeder RG (2004) E protein silencing by the leukemogenic AML1-ETO fusion protein. *Science* 305:1286–1289.
3. Bodenhausen G, Ruben D (1980) Natural abundance ^{15}N NMR by enhanced heteronuclear spectroscopy. *Chem Phys Lett* 69:185–189.
4. Kay LE, Ikura M, Tschudin R, Bax A (1990) 3-Dimensional triple-resonance NMR-spectroscopy of isotopically enriched proteins. *J Magn Reson* 89:496–514.
5. Wang AC, et al. (1994) An efficient triple-resonance experiment for proton-directed sequential backbone assignment of medium-sized proteins. *J Magn Reson B* 105: 196–198.
6. Grzesiek S, Bax A (1993) Amino acid type determination in the sequential assignment procedure of uniformly 13C/15N-enriched proteins. *J Biomol NMR* 3:185–204.
7. Ikura M, Kay LE, Bax A (1991) Improved three-dimensional 1H-13C-1H correlation spectroscopy of a 13C-labeled protein using constant-time evolution. *J Biomol NMR* 1: 299–304.
8. Nietlispach D, et al. (1996) An approach to the structure determination of larger proteins using triple resonance NMR experiments in conjunction with random fractional deuteration. *J Am Chem Soc* 118:407–415.
9. Ikura M, et al. (1991) Secondary structure and side-chain 1H and 13C resonance assignments of calmodulin in solution by heteronuclear multidimensional NMR spectroscopy. *Biochemistry* 30:9216–9228.
10. Kay LE, Xu GY, Singer AU, Muhandiram DR, Forman-Kay JD (1993) A gradient-enhanced HCCH-TOCSY experiment for recording sidechain 1H and 13C correlations in H2O samples of proteins. *J Magn Reson* 101B:333–337.
11. Yamazaki T, Forman-Kay JD, Kay LE (1994) Two-dimensional NMR experiments for correlating 13Cbeta and 1Hdelta/epslon chemical shifts of aromatic residues in 13C-labeled proteins via scalar couplings. *J Am Chem Soc* 115:11054–11055.
12. Zhang O, Kay LE, Olivier JP, Forman-Kay JD (1994) Backbone 1H and 15N resonance assignments of the N-terminal SH3 domain of drk in folded and unfolded states using enhanced-sensitivity pulsed field gradient NMR techniques. *J Biomol NMR* 4: 845–858.

13. Muhandiram DR, Farrow NA, Xu GY, Smallcombe SH, Kay LE (1993) A gradient 13C NOESY-HSQC experiment for recording NOESY spectra of 13C-labeled proteins dissolved in H2O. *J Magn Reson* 102B:317–321.
14. Zwahlen C, et al. (1997) Methods for measurement of intermolecular NOEs by multinuclear NMR spectroscopy: Application to a bacteriophage λ N-peptide/boxB RNA complex. *J Am Chem Soc* 119:6711–6721.
15. Delaglio F, et al. (1995) NMRPipe: A multidimensional spectral processing system based on UNIX pipes. *J Biomol NMR* 6:277–293.
16. Johnson BA (2004) Using NMRView to visualize and analyze the NMR spectra of macromolecules. *Methods Mol Biol* 278:313–352.
17. Bartels C, Xia T, Billeter M, Guntert P, Wuthrich K (1995) The program XEASY for computer-supported NMR spectral analysis of biological macromolecules. *J Biomol NMR* 6:1–10.
18. López-Méndez B, Güntert P (2006) Automated protein structure determination from NMR spectra. *J Am Chem Soc* 128:13112–13122.
19. Shen Y, Delaglio F, Cornilescu G, Bax A (2009) TALOS+: a hybrid method for predicting protein backbone torsion angles from NMR chemical shifts. *J Biomol NMR* 44:213–223.
20. Wishart DS, Sykes BD (1994) The 13C chemical-shift index: A simple method for the identification of protein secondary structure using 13C chemical-shift data. *J Biomol NMR* 4:171–180.
21. Kasper LH, et al. (2002) A transcription-factor-binding surface of coactivator p300 is required for haematopoiesis. *Nature* 419:738–743.
22. Nederveen AJ, et al. (2005) RECOORD: A recalculated coordinate database of 500+ proteins from the PDB using restraints from the BioMagResBank. *Proteins* 59:662–672.
23. Laskowski RA, Rullmannn JA, MacArthur MW, Kaptein R, Thornton JM (1996) AQUA and PROCHECK-NMR: Programs for checking the quality of protein structures solved by NMR. *J Biomol NMR* 8:477–486.
24. You H, et al. (2006) FOXO3a-dependent regulation of Puma in response to cytokine/growth factor withdrawal. *J Exp Med* 203:1657–1663.
25. You H, Yamamoto K, Mak TW (2006) Regulation of transactivation-independent proapoptotic activity of p53 by FOXO3a. *Proc Natl Acad Sci USA* 103:9051–9056.

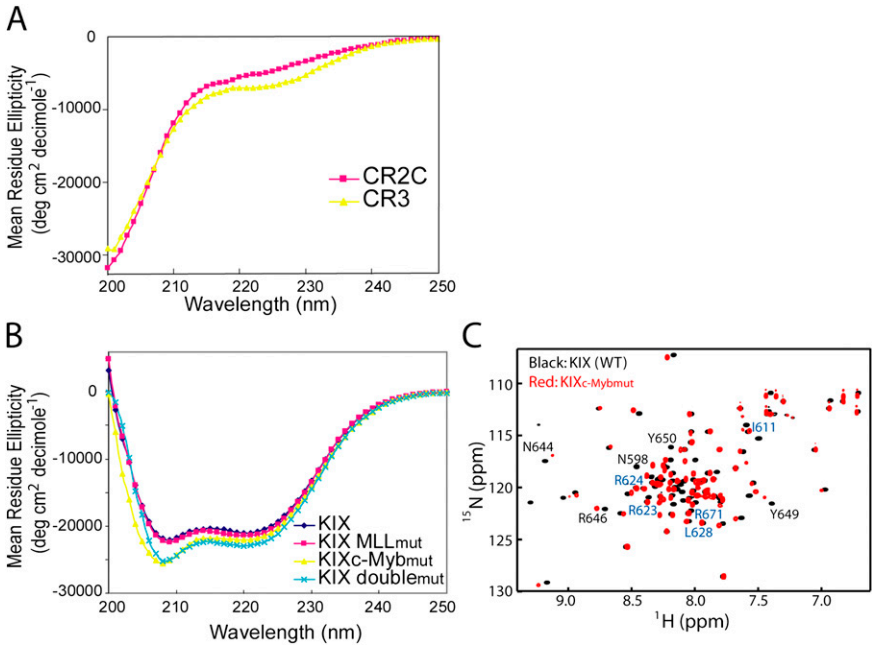

Fig. S1. Structural characterization of FOXO3a TADs and KIX mutants. (*A*) CR2C and CR3 are unstructured in solution. CD spectra of isolated CR2C and CR3 are shown in red and yellow, respectively. (*B*) KIX mutations do not disrupt folding. CD spectra of WT KIX and the mutants MLL_{mut} (I660A and L664A), c-Myb_{mut} (A654Q, Y650A, and Y658A), and $double_{mut}$ (A654Q, Y650A, Y658A, I660A, and L664A) are overlaid. (*C*) HSQC spectra of WT KIX (black) and $KIX_{c\text{-}Mybmut}$ (red) are overlaid. Residues that exhibit a large chemical shift change in the mutant (labeled in black) are located in the immediate vicinity of one of the three mutations. Note that peaks from residues in the MLL site (labeled blue) were not perturbed by mutation of the c-Myb site.

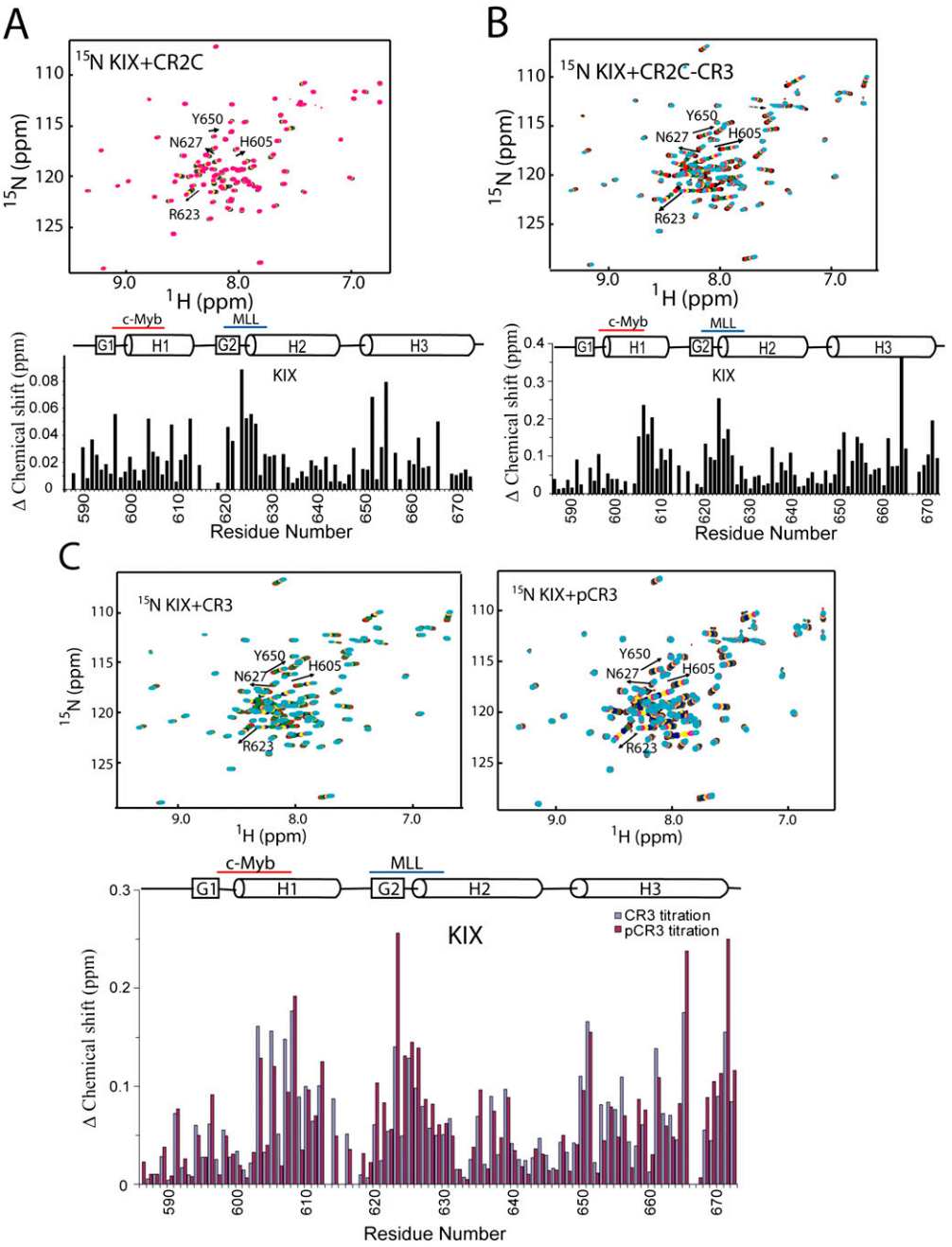

Fig. S2. NMR titrations of KIX with FOXO3a peptides. (*A*) Titration of ^{15}N-labeled KIX with unlabeled CR2C peptide. HSQC spectra of ^{15}N-labeled KIX with increasing concentrations of CR2C peptide (0- to 2.5-fold excess) are overlaid. (*B*) Titration of ^{15}N-labeled KIX with unlabeled CR2C-CR3 peptide. HSQC spectra of ^{15}N-labeled KIX with increasing concentrations of CR2C-CR3 peptide (0- to 3.5-fold excess) are overlaid. (*C*) Effect of phosphorylation on CR3 binding to KIX. (*Upper Left*) Overlaid HSQC spectra of ^{15}N-labeled KIX titrated with unlabeled CR3 peptide (0- to 2.5-fold excess). (*Upper Right*) Overlaid HSQC spectra of ^{15}N-labeled KIX titrated with unlabeled CR3 peptide phosphorylated on Serine 626 (pCR3, 0- to 2-fold excess). (*Lower*) Chemical shift change (calculated as $\sqrt{[(\Delta H)^2 + (\Delta N/6.5)^2]}$) at the titration end point for each KIX residue. KIX regions that form a distinct part of the c-Myb site (N terminus of H1) or the MLL site (G2 and N termini of H2) are indicated above with the secondary structural elements of KIX.

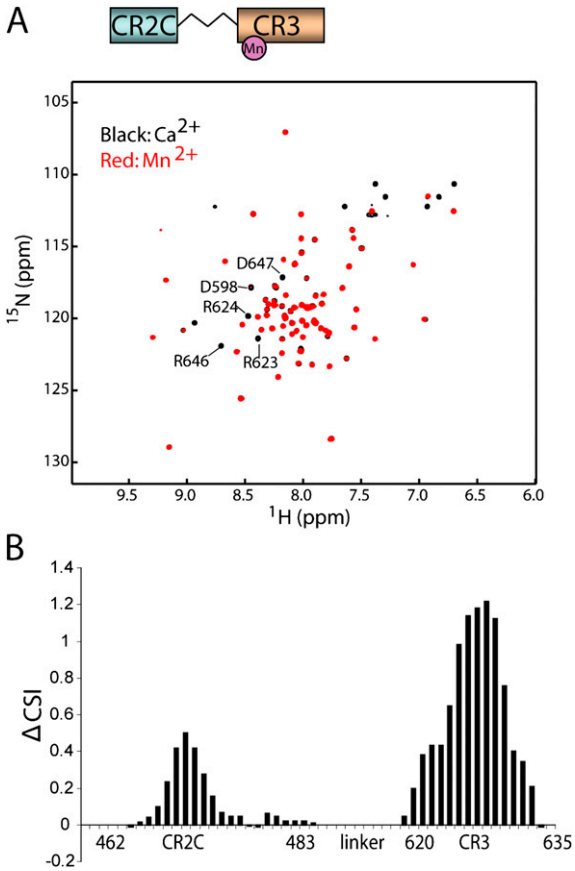

Fig. S3. NMR characterization of CR2C-CR3 binding to KIX. (*A*) Mapping the CR3 binding site on KIX by PRE. A thiol-reactive EDTA tag was covalently linked to C622 in the N terminus of CR3 and used to chelate Ca^{2+} (diamagnetic) or Mn^{2+} (paramagnetic). The overlaid HSQC spectra of ^{15}N-labeled KIX plus CR2C-CR3-EDTA in the presence of Ca^{2+} (black) and Mn^{2+} (red) are shown. The most severely broadened backbone resonances are labeled, and these residues are highlighted in the KIX structure in Fig. S5 *C* and *D*. The ratio of KIX to CR2C-CR3-EDTA peptide was ~2:1 in both the Ca^{2+} and Mn^{2+} conditions. (*B*) KIX binding increases the helicity of CR2C and CR3. The change in chemical shift index value (1) of CR2C-CR3 on KIX binding ($\Delta CSI = CSI_{bound} - CSI_{free}$) is plotted for each residue. Positive ΔCSI values indicate increased helicity.

1. Wishart DS, Sykes BD (1994) The 13C chemical-shift index: A simple method for the identification of protein secondary structure using 13C chemical-shift data. *J Biomol NMR* 4:171–180.

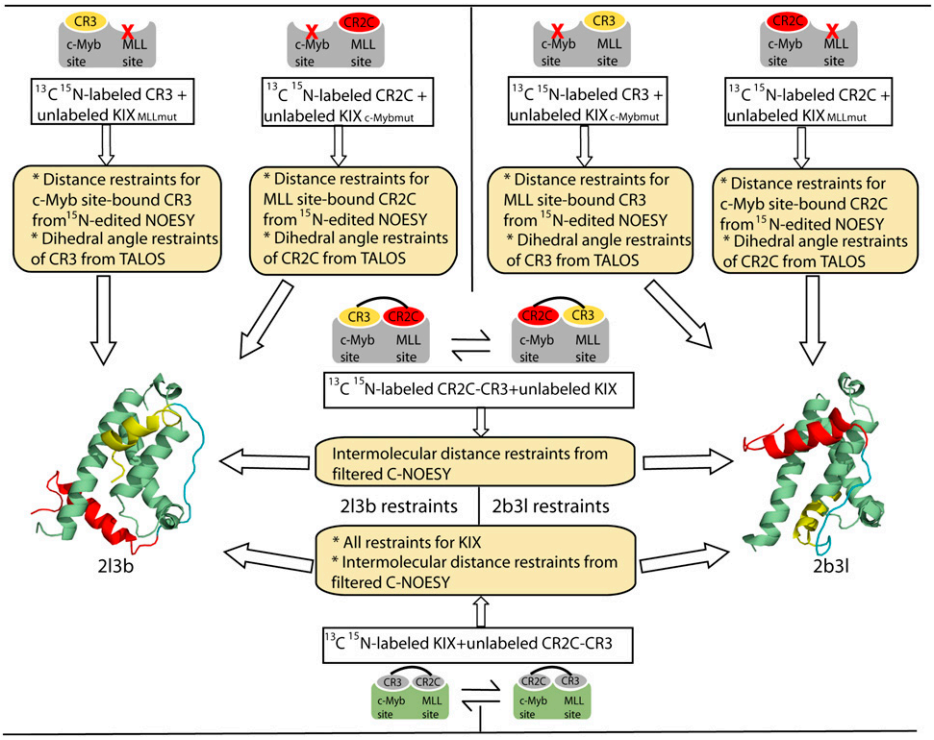

Fig. S4. Strategy for determining NMR structures of two conformations of the CR2C-CR3–KIX complex. Labeling schemes and constructs used are indicated in the cartoons. Gray indicates unlabeled proteins, colors indicate ^{13}C ^{15}N-labeled proteins, and red crosses indicate mutated binding sites. Yellow boxes indicate the NMR experiments collected with each sample and the restraints obtained for the structure calculation. In the 2l3b conformation, CR2C is bound to the MLL site and CR3 is bound to the c-Myb site, whereas in the 2b3l conformation, CR2C is bound to the c-Myb site and CR3 is bound to the MLL site. Further details are provided in *SI Methods*.

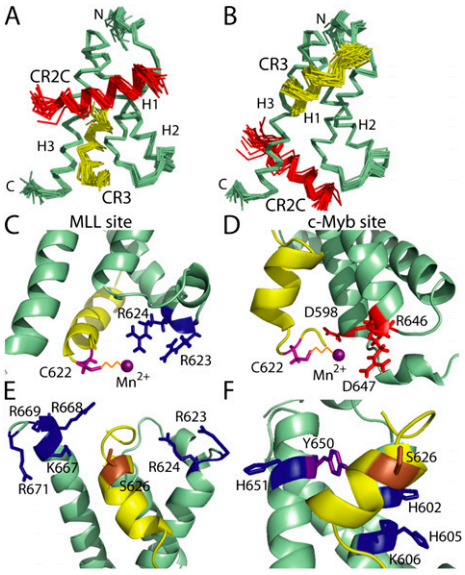

Fig. S5. Structures of KIX in complex with FOXO3a CR2C-CR3. The 20-structure ensembles of CR2C-CR3 are bound to KIX in the 2b3l conformation (*A*) and 2l3b conformation (*B*). KIX is shown in green, CR2C is shown in red, and CR3 is shown in yellow. Ribbon diagrams illustrate CR3 in the MLL site (*C*) and in the c-Myb site (*D*). The side chain of residue C622 is labeled and colored in purple, the EDTA tag and Mn^{2+} cation that were attached to this residue are shown in cartoon form, and the residues that were most affected by PRE are colored red in the c-Myb site and blue in the MLL site. The location of the AMPK phosphorylation target residue S626 in KIX complexes is shown. Ribbon diagrams of CR3 in the MLL site (*E*) and in the c-Myb site (*F*) are shown with the side chain of S626 colored brown and the side chains of KIX residues with potential to interact with the phosphate group displayed in blue (basic residues) and purple (hydrophobic residue).

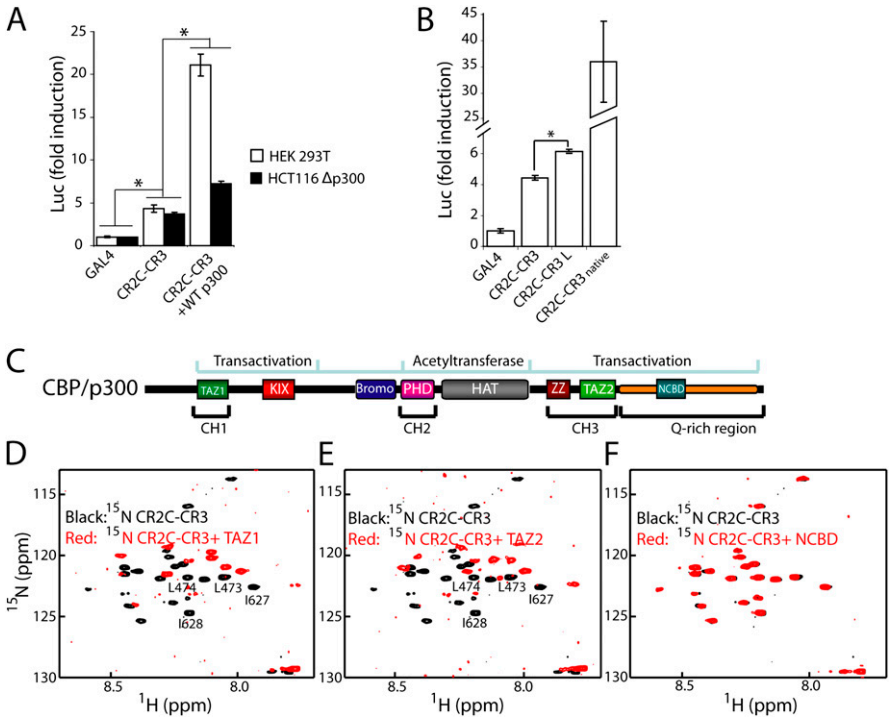

Fig. S6. FOXO3a CR2C-CR3 mediates transactivation through interactions with TAZ1/2 as well as the KIX domains of CBP/p300. (*A*) FOXO3a CR2C-CR3 activates the luciferase gene. Expression of luciferase from a plasmid under the control of a promoter containing five GAL4 binding sites was assayed in two cell types expressing GAL4 DBD or GAL4 DBD-CR2C-CR3 with or without exogenous p300 expression. White bars indicate HEK 293T cells, and black bars indicate HCT116 Δp300 cells. $*P < 0.01$. (*B*) Dependence of transactivation activity of tandem TADs on linker. Luciferase expression was assayed in HEK 293T cells expressing GAL4 DBD or GAL4 DBD fused to CR2C-CR3 [linked by $(GGGS)_3$], CR2C-CR3L [linked by $(GGGS)_9$], or CR2C-$CR3_{native}$ (linked by native sequence of ~150 residues). Luciferase activity was normalized to that of GAL4 DBD alone. $*P < 0.01$. All experiments were repeated three times, and the data are presented as mean ± SEM. (*C*) Domain architecture of CBP/p300. The conserved domains are labeled, and their functions are shown above. (*D–F*) Probing CBP/p300 TADs for interaction with CR2C-CR3. Overlaid spectra of ^{15}N-labeled CR2C-CR3 alone (black) and in the presence of a twofold excess of unlabeled TAZ1 (*D*), TAZ2 (*E*), and NCBD (*F*) (each shown in red).

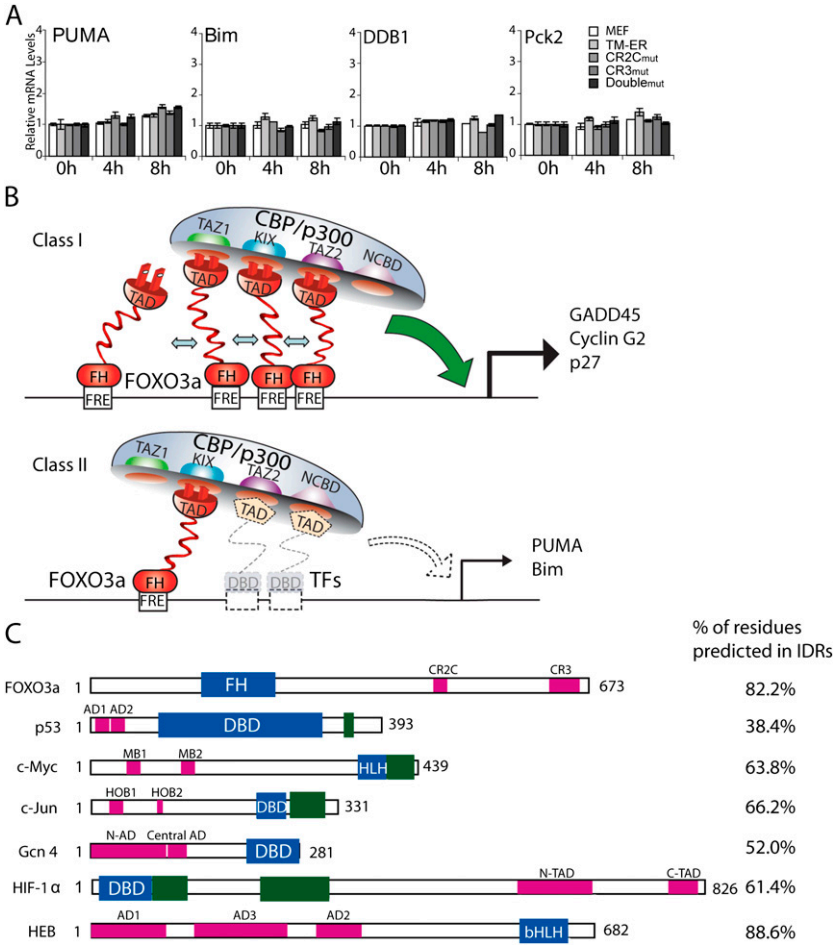

Fig. S7. Role of CR2C and CR3 in transactivation of endogenous target genes by full-length FOXO3a: model of multivalent binding and relevance to other transcription factors. (*A*) MEF cells were stably transformed with FOXO3aTM-ER bearing WT or mutated CR2C and/or CR3 regions. After activation of FOXO3a in each cell line by 4-OHT treatment, the mRNA levels of FOXO3a target genes were examined and normalized to the basal level determined before 4-OHT treatment. All experiments were repeated three times, and the data are shown as mean ± SEM. Data for genes that did not respond to FOXO3aTM-ER under the conditions of our assay are presented here, whereas those genes that were up-regulated by FOXO3aTM-ER are shown in Fig. 5. (*B*) Multivalent binding model of CBP/p300 recruitment by FOXO3a. The system is represented by an "electrical plug and receptacle" model, in which the FOXO3a TAD, comprising both CR2C and CR3, is the plug; the TADs of CBP/p300 are the receptacles; the IDR is the flexible cord; and FH is anchored to the FRE in the promoter. (*Upper*) Promoter regions of many FOXO3a target genes, including GADD45, Cyclin G2, and p27, which were up-regulated by FOXO3a in our RT-PCR assay (Fig. 5), contain multiple FREs. In addition, we have identified four FOXO3a binding sites on CBP/p300 (KIX c-Myb, KIX MLL, TAZ1, and TAZ2). Enrichment of FOXO3a at promoters bearing multiple FREs would allow the formation of multivalent interactions between the CR2C and CR3 TAD regions of FOXO3a and CBP/p300. Each TAD interacts weakly with CBP/p300; however, the product of multiple weak binding events would stabilize the interaction, promoting recruitment and initiation of gene transcription (represented by the solid arrow). (*Lower*) FOXO3a target genes, such as PUMA, with only a single FRE in their promoters were not activated by FOXO3a in our experimental system. The transient interaction between a single FOXO3a molecule and CBP/p300 may not be sufficient to support initiation of transcription (represented by the broken arrow). Promoters with a single FRE often contain additional recognition elements for other transcription factors (TFs), and substantial transcriptional activation requires the cooperation of multiple transcription factors. For example, the PUMA promoter contains one FRE and two p53 binding sites (1, 2), and effective up-regulation may require both FOXO3a and p53. Thus, we propose that FOXO3a target genes may be divided into two classes. Genes that are up-regulated when active FOXO3a is localized to the nucleus are designated class I, and generally have multiple FREs. FOXO3a alone is not sufficient to activate class II genes, which often contain a single FRE and have more stringent requirements for gene activation, such as coactivation or colocalization of other transcriptional activators, which function cooperatively with FOXO3a through diverse mechanisms (reviewed in 3). The invariant long IDRs that link the FH domain and the TADs (CR2C and CR3) enable FOXO3a to change orientation relatively freely, and hence to adapt to position the coactivator CBP/p300 correctly on the chromosome or interact with additional transcription factors and coregulators. This architecture is conserved in all FOXO genes. (*C*) Tandem TADs located in extended IDRs are a common feature in transcription factors. DNA binding domains are shown as blue boxes, other structured domains are indicated as green boxes, and TADs are labeled and colored purple. The percentage of each transcription factor that is intrinsically disordered (predicted by DISOPRED2) (*4*) is indicated.

1. You H, et al. (2006) FOXO3a-dependent regulation of Puma in response to cytokine/growth factor withdrawal. *J Exp Med* 203:1657–1663.
2. Wang P, Yu J, Zhang L (2007) The nuclear function of p53 is required for PUMA-mediated apoptosis induced by DNA damage. *Proc Natl Acad Sci USA* 104:4054–4059.
3. van der Vos KE, Coffer PJ (2008) FOXO-binding partners: It takes two to tango. *Oncogene* 27:2289–2299.
4. Ward JJ, Sodhi JS, McGuffin LJ, Buxton BF, Jones DT (2004) Prediction and functional analysis of native disorder in proteins from the three kingdoms of life. *J Mol Biol* 337:635–645.

Table S1. Dissociation constants (K_d) for the interactions between FOXO3a TAD peptides and their mutants with CBP/p300 TADs

	KIX	TAZ1	TAZ2
CR2C	>500	NA	NA
CR2C-CR3$_{native}$	97 ± 40	NA	NA
CR2C$_{mut}$	NBD	NBD	NBD
CR3$_{Trpmut}$	NBD	ND	ND

K_d values (μM) were determined by ITC. NBD, no binding detected, indicating any interaction is too weak to be detected by ITC; ND, not determined, indicating weak binding was detected by ITC, but the K_d value could not be determined; NA, not available, indicating the experiment was not performed.

Table S2. Structural statistics of KIX:CR2C–CR3 complexes

	CR2C-CR3	2b3l	KIX	2l3b	CR2C-CR3
NMR distance and dihedral constraints					
Distance constraints					
Total NOE	187		2,434		196
Intraresidue	76		494		91
Sequential	81		637		90
Middle-range, 1<|I − j|<5	30		845		15
Long-range, |I − j|≥5	0		458		0
Hydrogen bonds, upper/lower	13 × 2		46 × 2		13 × 2
Total dihedral angle restraints	52		92		50
Intermolecular NOE		74		100	
Structure statistics					
Restraints violations					
Distance, >0.3 Å		0.1		0.35	
Dihedral, >5°		0		0.05	
Maximum distance constraints violation, Å		0.33		0.35	
Distance constraints rmsd, Å		0.017 ± 0.001		0.019 ± 0.001	
Dihedral angle constraints rmsd, °		0.31 ± 0.05		0.34 ± 0.07	
Average pairwise rmsd, Å					
Heavy		2.2 ± 0.5		2.2 ± 0.7	
Backbone		2.1 ± 0.7		2.1 ± 0.9	
Ordered region*, Å					
Heavy		0.98 ± 0.08		1.04 ± 0.09	
Backbone		0.54 ± 0.08		0.59 ± 0.12	
Ramachandran plot (ordered region*), %					
Most favored regions		96.3		94.7	
Additional allowed regions		3.7		5.2	
Generously allowed regions		0		0.1	
Disallowed regions		0		0	

The distance constraints for each conformation of CR2C-CR3 are indicated in separated columns, as are the intermolecular NOEs. *For 2b3l, the ordered regions are as follows: KIX R588-R669, FOXO3a CR2C N467-H481, and CR3 M624-D634. For 2l3b, the ordered regions are as follows: KIX R588-R669, FOXO3a CR2C Q468-S480, and CR3 L620-M633.